

Meta-AF: Meta-Learning for Adaptive Filters

Jonah Casebeer, *Student Member, IEEE*, Nicholas J. Bryan, *Member, IEEE*, Paris Smaragdis, *Fellow, IEEE*

Abstract—Adaptive filtering algorithms are pervasive throughout modern society and have had a significant impact on a wide variety of domains including audio processing, telecommunications, biomedical sensing, astrophysics and cosmology, seismology, and many more. Adaptive filters typically operate via specialized online, iterative optimization methods such as least-mean squares or recursive least squares and aim to process signals in unknown or nonstationary environments. Such algorithms, however, can be slow and laborious to develop, require domain expertise to create, and necessitate mathematical insight for improvement. In this work, we seek to go beyond the limits of human-derived adaptive filter algorithms and present a comprehensive framework for learning online, adaptive signal processing algorithms or update rules directly from data. To do so, we frame the development of adaptive filters as a meta-learning problem in the context of deep learning and use a form of self-supervision to learn online iterative update rules for adaptive filters. To demonstrate our approach, we focus on audio applications and systematically develop meta-learned adaptive filters for five canonical audio problems including system identification, acoustic echo cancellation, blind equalization, multi-channel dereverberation, and beamforming. For each application, we compare against common baselines and/or current state-of-the-art methods and show we can learn high-performing adaptive filters that operate in real-time and, in most cases, significantly outperform all past specially developed methods for each task using a single general-purpose configuration of our method.

Index Terms—adaptive filtering, meta learning, online optimization, learning to learn, deep learning

I. INTRODUCTION

ADAPTIVE signal processing and adaptive filter theory are cornerstones of modern signal processing and have had a deep and significant impact on modern society. Applications of adaptive filters (AF) include audio processing, telecommunications, biomedical sensing, astrophysics and cosmology, seismology and more. Audio applications, in particular, are of exceptional importance and find utility for many problems such as single- and multi-channel system identification, echo cancellation, prediction, dereverberation, beamforming, noise cancellation, and beyond. AFs typically operate via online iterative optimization methods, such as least mean square filtering (LMS), normalized LMS (NLMS), recursive least-squares (RLS), or Kalman filtering (KF), to solve streaming, online, optimization problems over time [1]–[6] to process signals in unknown and/or nonstationary environments.

J. Casebeer is with the Department of Computer Science, University of Illinois at Urbana-Champaign, Urbana, IL 61801 USA (e-mail: jonahmc2@illinois.edu). Work performed in part interning at Adobe Research. N. J. Bryan was the lead advisor for this work and is with Adobe Research, San Francisco, CA, 94103 USA (e-mail: njb@ieee.org). P. Smaragdis is with the Department of Computer Science and Department, University of Illinois at Urbana-Champaign, Urbana, IL 61801 USA (e-mail: paris@illinois.edu) Partially funded by NIFA award #2020-67021-32799

Manuscript received Month Day, Year; revised Month Day, Year.

AF tasks are often categorized into one of four core categories: system identification, inverse modeling, prediction, or interference cancellation [4]. Each of these categories has numerous AF applications, so advances in one category or application can often be applied to many others. In the audio domain, acoustic echo cancellation (AEC) can be formulated as single- or multi-channel system identification and has been studied extensively [7]–[16]. Equalization can be formulated as an inverse modeling problem, has been explored in single- and multi-channel formats, and is particularly useful for sound zone reproduction and active noise control [17]–[22]. Dereverberation can be formulated as a prediction problem and has been studied considerably in this format [23]–[29]. Finally, multi-microphone enhancement or beamforming can be formulated as an informed interference cancellation task and also has a breadth of associated algorithms [30]–[36].

When we consider AFs in the context of deep neural networks (DNNs), we note two main observations. First, AFs continue to be used extensively, but mostly in hybrid approaches that combine neural networks with standard AF algorithms. Second, the underlying algorithms for AFs themselves have had little change in several decades. Hybrid approaches, however, have proven very successful. For a variety of AEC tasks [37]–[45], for example, neural networks are used for residual echo suppression, noise suppression, or related. In a similar vein, neural networks paired with AFs for active noise control tasks have proven successful [46]–[49]. For dereverberation, DNNs have proven useful for both online and offline approaches by directly estimating statistics of the dereverberated speech [50]–[54]. This pattern has repeated itself for beamforming applications, where DNNs have proven vital and have led to many performance improvements [55]–[58]. In many of these works, DNNs are trained to predict ratio-masks, or otherwise directly enhance/separate the desired signal. In essence, they act as a distinct module within a larger pipeline that also uses AFs.

In contrast, there are a small number of works that more tightly couple neural networks and AFs and use DNNs for optimal control of AFs. Recently, it was shown that DNNs can estimate statistics to control step-sizes [59] or estimate entire updates [60] for a single-channel AEC. Similarly, past work has used DNNs to predict updates for the internal statistics of multi-channel beamformers [61] and to learn source-models for multi-channel source separation [62]. These works differ from hybrid approaches in that they leverage neural networks to update or control AFs directly and thus focus on improving the performance of AFs themselves. Such improvement can be leveraged in isolation or, in theory, together with complementary hybrid approaches.

More broadly, the idea of controlling AFs via neural networks is related to several disciplines of signal processing

and machine learning including optimal control, optimization, automatic machine learning, reinforcement learning and meta-learning. Relevant works within these areas include automatic selection of step sizes [7], [63], [64], the direct control of model weights [65]–[67], rapid fine-tuning [68], and meta-learning optimization rules [69]. Out of these works, learning optimization rules or *learned optimizers* is of critical relevance [70]–[72] and presents the idea of using one neural network as a function that optimizes another function. Such works, however, focus on creating learned optimizers for training neural networks in an offline setting, where the latter network is the final product, and the learned optimizer is otherwise discarded (or otherwise used to train additional networks). Moreover, this work has had little application to AFs, except for our own work [60], which we extend here.

In this work, we formulate the development of AF algorithms as a meta-learning problem. We then learn adaptive filter update rules directly from data using a form of self-supervision together with truncated backpropagation through time (TBPTT). We call our approach meta adaptive filtering (Meta-AF) and do so to communicate the idea that we meta-learn AF algorithms from data, no longer need humans to hand-derive update equations, do not need any supervised labeled data for learning, and do not need exhaustive tuning. To showcase our approach, we systematically develop learned AFs for exemplary applications of each of the four canonical AF architectures. Then, for each AF task, we compare our work to a suite of baselines and/or state-of-the-art approaches for the problems of system identification, acoustic echo cancellation, equalization, single- and multi-channel dereverberation, and multi-channel interference cancellation (beamforming). For all tasks, we use identical hyper-parameters, significantly reducing engineering and design time. We evaluate performance using signal-to-noise ratio (SNR)-like signal level metrics and perceptual or task specific metrics as well as specific qualitative comparisons. Our results show we can learn high-quality AF algorithms that, in most cases, significantly outperform past specially developed methods.

The contributions of our work are as follows: 1) We present the first general purpose method of meta-learning AF algorithms (update rules) directly from data via self-supervision (no labels required). 2) We apply our approach to all canonical AF architecture categories including system identification, inverse modeling, prediction, and (informed) interference cancellation. 3) We show how a single hyper-parameter configuration of our approach, trained with different datasets and losses, can outperform all common AF baselines and/or several past state-of-the-art methods according to one or more evaluation metrics and are suitable for real-time operation on commodity hardware. Compared to our previous work on AEC in single-talk [60], we present several new core contributions including core algorithmic improvements and extensive validation across tasks. We release demos for each task and open source code¹, including all baselines, creating an extensive resource for AFs.

II. BACKGROUND

A. Variables and Notation

We represent multi-channel time-domain signal vectors via underlined bold lowercase letters and use bracket indexing $[\tau]$ to denote if it is time-varying. For example, $\underline{\mathbf{u}}[\tau] = (\underline{u}[\tau R - N + 1], \dots, \underline{u}[\tau R]) \in \mathbb{R}^{N \times M}$ is a time-domain signal, where N is the window length in samples, M is the number of channels, τ is the time index within the context of a longer signal, R is the hop size in samples, and $N - R$ samples is the overlap between frames. We represent frequency-domain signals without the underline. For example, $\mathbf{u}[\tau] \in \mathbb{C}^{K \times M}$ is a frequency-domain signal with K frequency bins, M channels at time τ . We index frequency-domain vector rows via the subscript k , columns via the subscript m , and elements via the subscripts km . We represent a buffer of B frames at frequency k as the concatenation, $\tilde{\mathbf{u}}_k[\tau] = [\mathbf{u}_k[\tau - B + 1], \dots, \mathbf{u}_k[\tau]] \in \mathbb{C}^{BM}$, and index buffered rows via the subscript b . In all AF tasks, we use $\mathbf{u}[\tau]$ to represent the AF input, $\mathbf{d}[\tau]$ to represent the target or desired response, $\mathbf{y}[\tau]$ to represent the estimated response and, when applicable, $\mathbf{s}[\tau]$ to represent the true desired signal. We use $*$ to denote convolution, \odot to denote element-wise multiplication, $^\top$ to denote the transpose, H to denote the Hermitian transpose, $\text{diag}(\cdot)$ to represent the conversion of a vector to a diagonal matrix, $\text{cat}(\dots)$ to represent concatenation, and E for the expected value. The matrix \mathbf{F}_N is the N -point Discrete Fourier transform (DFT) matrix, \mathbf{I}_N is the $N \times N$ identity matrix, $\mathbf{0}_{N \times R}$ is an $N \times R$ matrix of zeros, and $\mathbf{1}_{N \times R}$ is an $N \times R$ matrix of ones.

B. Overlap-Save & Overlap-Add Filtering

We perform short-time (STFT) Fourier filtering using either overlap-save (OLS) or overlap-add (OLA) style convolution. The OLS method uses block processing by splitting the input signal into overlapping windows and recombines complete non-overlapping components. Given a frequency domain signal, $\mathbf{u}_m[\tau] \in \mathbb{C}^K$, and a frequency domain filter $\mathbf{w}_m[\tau] \in \mathbb{C}^K$, the frequency and time output for the m^{th} channel, respectively are

$$\mathbf{y}_m[\tau] = \text{diag}(\mathbf{u}_m[\tau])\mathbf{Z}_w\mathbf{w}_m[\tau] \in \mathbb{C}^K \quad (1)$$

$$\underline{\mathbf{y}}_m[\tau] = \mathbf{Z}_y\mathbf{y}_m[\tau] \in \mathbb{R}^R \quad (2)$$

where $\mathbf{Z}_w = \mathbf{F}_K\mathbf{T}_R^\top\mathbf{T}_R\mathbf{F}_K^{-1} \in \mathbb{C}^{K \times K}$ and $\mathbf{Z}_y = \bar{\mathbf{T}}_R\mathbf{F}_K^{-1} \in \mathbb{C}^{R \times K}$ are anti-aliasing matrices, $\mathbf{T}_R = [\mathbf{I}_{K-R}, \mathbf{0}_{K-R \times R}] \in \mathbb{R}^{K-R \times K}$ trims the last R samples from a vector and $\bar{\mathbf{T}}_R = [\mathbf{0}_{K-R \times R}, \mathbf{I}_{K-R}] \in \mathbb{R}^{K-R \times K}$ trims the first R samples.

The counterpart to OLS is OLA filtering, which computes the frequency and time output, and buffer update as

$$\mathbf{y}_m[\tau] = \text{diag}(\mathbf{u}_m[\tau])\mathbf{w}_m[\tau] \in \mathbb{C}^K \quad (3)$$

$$\underline{\mathbf{y}}_m[\tau] = \mathbf{T}_R\mathbf{F}_K^{-1}\mathbf{y}_m[\tau] + \bar{\mathbf{T}}_R\mathbf{b}_m[\tau - 1] \in \mathbb{R}^R \quad (4)$$

$$\mathbf{b}_m[\tau] = \mathbf{F}_K^{-1}\mathbf{y}_m[\tau] + \mathbf{T}_R^\top\bar{\mathbf{T}}_R\mathbf{b}_m[\tau - 1] \in \mathbb{C}^K. \quad (5)$$

Typically, the forward and inverse DFTs are combined with analysis and synthesis windows and optionally zero-padded. We use Hann windows [73]. For multi-frame frequency-domain filters, the (anti-aliased) filter is $\mathbf{w}_m[\tau] \in \mathbb{C}^{K \times BM}$ with B buffered frequency frames, the stacked input is $\tilde{\mathbf{u}}[\tau] \in \mathbb{C}^{K \times BM}$, and the output is $\mathbf{y}_m[\tau] = (\tilde{\mathbf{u}}[\tau] \odot \mathbf{w}_m[\tau])\mathbf{1}_{BM \times 1}$.

¹Please see: <https://jmcasbeer.github.io/projects/metaaf>

C. Adaptive Filter Problem Formulation

We define an AF as an algorithm or optimizer that solves

$$\hat{\theta}[\tau] = \arg \min_{\theta[\tau]} \mathcal{L}(\cdots)[\tau] \quad (6)$$

via an additive update rule of the form

$$\theta[\tau + 1] = \theta[\tau] + \Delta[\tau], \quad (7)$$

where $\mathcal{L}(\cdots)[\tau]$ or $\mathcal{L}(\cdots)$ for short is the loss at time τ , $\theta[\tau]$ are the filter parameters at time τ , and $\Delta[\tau]$ is the update. Common losses include the mean-square error (MSE),

$$\mathcal{L}_{MSE}[\tau] = E[|\mathbf{e}_m[\tau]|^2] = E[|\mathbf{d}_m[\tau] - \mathbf{y}_m[\tau]|^2], \quad (8)$$

the instantaneous square error (ISE),

$$\mathcal{L}_{ISE}[\tau] = |\mathbf{e}_m[\tau]|^2 = |\mathbf{d}_m[\tau] - \mathbf{y}_m[\tau]|^2, \quad (9)$$

and the weighted least squares error (WSE),

$$\mathcal{L}_{WSE}[\tau] = \sum_{n=0}^{\tau} \gamma^{\tau-n} |\mathbf{d}_m[n] - \mathbf{y}_m[n]|^2, \quad (10)$$

where γ is a forgetting factor and the output \mathbf{y} is computed via (1) or (3) for frequency-domain signals or losses and (2) or (4) for time-domain signals or losses.

D. Conventional Optimizers

For audio AFs, it is common to leverage OLS or OLA filtering and solve (6) via optimization methods per frequency bin. So, we modify (7) to be

$$\theta_k[\tau + 1] = \theta_k[\tau] + \Delta_k[\tau], \quad (11)$$

where the update $\Delta_k[\tau]$ is per frequency k . We review four relevant conventional AF optimizers in this form below.

1) *Least Mean Square*: The least mean square optimizer (LMS) optimizer is a stochastic gradient descent method that uses the ISE loss and gradient. The LMS update is

$$\Delta_k[\tau] = -\lambda \nabla_k[\tau], \quad (12)$$

where λ is the step-size and $\nabla_k[\tau]$ is the gradient of the ISE. Note LMS is stateless and only a function of the gradient.

2) *Normalized Least Mean Square*: The normalized LMS (NLMS) algorithm modifies LMS via a running normalizer based on the input signal power. The NLMS update is

$$v_k[\tau] = \gamma v_k[\tau - 1] + (1 - \gamma) \|\mathbf{u}_k[\tau]\|^2 \quad (13)$$

$$\Delta_k[\tau] = -\lambda \frac{\nabla_k[\tau]}{v_k[\tau]}, \quad (14)$$

where the division is element-wise, λ is the step-size and γ is a forgetting factor.

3) *Root Mean Squared Propagation*: The RMSProp optimizer [74] modifies NLMS by replacing $v_k[\tau]$ with a running per-element normalizer, $\nu[\tau]$ using forget factor γ as,

$$\nu_k[\tau] = \gamma \nu_k[\tau - 1] + (1 - \gamma) \|\nabla_k[\tau]\|^2 \quad (15)$$

$$\Delta_k[\tau] = -\lambda \frac{\nabla_k[\tau]}{\nu_k[\tau]}, \quad (16)$$

The value, $1/\sqrt{\nu_k[\tau]}$ supplements the fixed step-size λ and acts as an adaptive learning rate, $\lambda/\sqrt{\nu_k[\tau]}$. Compared to NLMS, the normalization factor here is computed from the gradient instead of the input signal power.

4) *Recursive Least Square*: The aim of the recursive least squares (RLS) algorithm is to exactly solve the AF loss, most commonly the WSE error. This is accomplished by expanding the weighted least squares error into a function of the weighted empirical signal covariance matrix, $\Phi_k = \sum_{\tau} \gamma^{N-\tau} \mathbf{u}_k[\tau] \mathbf{u}_k[\tau]^H$, and the (weighted) empirical cross-correlation vector $\mathbf{z}_k = \sum_{\tau} \gamma^{N-\tau} \mathbf{u}_k[\tau] \mathbf{d}_k[\tau]^H$ to compute the exact solution to the resulting normal equations, $\Phi_k \mathbf{w}_k = \mathbf{z}_k$, commonly with running estimates of Φ_k and \mathbf{z}_k . However, instead of performing repeated matrix inversion, the matrix inversion lemma is used. Thus, RLS can be implemented using a time-varying precision (inverse covariance) matrix $\mathbf{P}_k[t]$ and the Kalman-gain matrix $\mathbf{K}_k[t]$,

$$\mathbf{K}_k[\tau] = \frac{\mathbf{P}_k[\tau - 1] \mathbf{u}_k[\tau]}{\gamma + \mathbf{u}_k[\tau]^H \mathbf{P}_k[\tau - 1] \mathbf{u}_k[\tau]} \quad (17)$$

$$\mathbf{P}_k[\tau] = \frac{\mathbf{P}_k[\tau - 1] - \mathbf{K}_k[\tau] \mathbf{u}_k[\tau]^H \mathbf{P}_k[\tau - 1]}{\gamma} \quad (18)$$

$$\Delta_k[\tau] = \mathbf{K}_k[\tau] (\mathbf{d}_k[\tau] - \mathbf{y}_k[\tau])^H, \quad (19)$$

where γ is a forgetting factor and the initialization of $\mathbf{P}_k[\tau]$ is critical and should be based on the input SNR. Alternatively, QR decomposition techniques can be used [5].

When conventional optimizers are compared to each other, the order of performance commonly follows LMS, NLMS, RMSProp, and RLS, while the order of computational complexity is reversed. These algorithms, however, can be sensitive to tuning, nonstationarities, nonlinearities, and other issues that require engineering effort to mitigate failure cases. In this work, we exhaustively grid-search tune the hyperparameters on held-out validation sets of signals. Additionally, for the AEC task we compare against the uncertainty-aware Kalman filter optimizer [11] and open-source double-talk robust Speex algorithm [12]. For dereverberation, we compare to the NARA-WPE [28] model, a normalized RLS-based optimizer.

E. Related Work

Initial work on automatically tuning AFs has been explored in incremental delta-bar-delta [63], Autostep [64], and elsewhere. Recent machine learning literature discusses the idea of using DNNs to learn entirely novel optimizer update rules from scratch [69]–[72]. We take significant inspiration from this work, but make numerous advances specific to AFs. In particular, past learned optimizers [69] are element-wise, offline, real-valued, only a function of the gradient, and are trained to optimize general purposes neural networks. In contrast, we design *online* AF optimizers that use multiple input signals, are complex-valued, adapt block frequency-domain linear filters or similar, and integrate domain-specific insights to reduce complexity and improve performance (coupling across channels and time frames). Moreover, we deploy learned optimizers as the final output to solve one particular AF task at a time instead of using them to train downstream neural networks. We also note other promising work [59] which uses a supervised DNN to control the step-size of a Kalman filter for AEC. Compared to our work, we replace the entire update with a neural network, do not need supervisory signals, and apply techniques for a variety of tasks.

TABLE I: Relationship between conventional optimizers and our learnable neural network-based optimizer.

Optimizer	Inputs	State	Params	Update $\Delta_k[\tau]$
LMS	$\nabla_k[\tau]$	\emptyset	λ	(12)
NLMS	$\nabla_k[\tau], \mathbf{u}_k[\tau]$	$v_k[\tau]$	λ, γ	(14)
RMSProp	$\nabla_k[\tau]$	$\nu_k[\tau]$	λ, γ	(16)
RLS	$\mathbf{u}_k[\tau], \mathbf{d}_k[\tau], \mathbf{y}_k[\tau]$	$\mathbf{K}_k, \mathbf{P}_k$	γ	(19)
Ours	$\xi_k[\tau]$	$\psi_k[\tau]$	ϕ	g_ϕ

III. PROPOSED METHOD

A. Problem Formulation

We formulate AF algorithm design as a meta-learning problem and train neural networks to learn AFs from data, creating meta-learned adaptive filters. This is in contrast to typical AFs that are manually created by human engineers. To do so, we define a learned optimizer, $g_\phi(\cdot)$, as a neural network with one or more input signals parameterized by weights ϕ that iteratively optimizes an AF loss or *optimizee* $\mathcal{L}(\cdot, h_\theta(\cdot))$ or \mathcal{L} for short, using an additive update rule

$$\theta[\tau + 1] = \theta[\tau] + g_\phi(\cdot), \quad (20)$$

where \mathcal{L} receives one or more signals and is a function of a generalized filter $h_\theta(\cdot)$ parameterized by θ (e.g. linear filter).

We then seek an optimal AF optimizer $g_{\hat{\phi}}$ over dataset \mathcal{D}

$$g_{\hat{\phi}} = \arg \min_{g_\phi} E_{\mathcal{D}}[\mathcal{L}_M(g_\phi, \mathcal{L}(\cdot, h_\theta))], \quad (21)$$

where $\mathcal{L}_M(g_\phi, \mathcal{L}(\cdot, h_\theta))$ or \mathcal{L}_M for short, is the meta or optimizer loss that is a function of g_ϕ and AF loss \mathcal{L} and we drop (\cdot) for compactness. Intuitively, when we solve (21), we learn a neural network $g_\phi(\cdot)$ that when applied repeatedly via an additive update, solves the AF loss \mathcal{L} .

B. Optimizee Architecture & Loss

The optimizee, or the AF loss \mathcal{L} that is optimized via (20) is a function of the generalized filter or architecture $h_\theta(\cdot)$. The generalized filter can be any reasonable differentiable filtering operator such as time-domain FIR filters, lattice FIR filters, non-linear filters, frequency-domain filters, multi-delayed block frequency domain filters [3], etc. Similarly, the AF loss can be any reasonable differentiable loss such as the MSE, ISE, WSE, a regularized loss, negative log-likelihood, mutual information, etc. For our work, we focus on single- and multi-channel multi-frame linear block frequency-domain filters h_θ applied via OLS or OLA with parameters $\theta_k[\tau] = \{\mathbf{w}_k[\tau] \in \mathbb{C}^{M \times B}\}$ with M channels and B buffered frames per frequency k . We also set the AF loss $\mathcal{L}[\tau]$ to be the MSE over a single frame unless otherwise stated. Note, the MSE and typical AF losses do not need explicit train-time supervisory signals and thus can be considered self-supervised.

C. Optimizer Architecture & Loss

1) *Architecture*: Our optimizer g_ϕ is inspired by conventional AF optimizers such as LMS, NLMS, and RLS, but updated to have a neural network form. In particular, we focus on making a generalized, stochastic variant of an RLS-like

optimizer that is applied independently per frequency k to our optimizee parameters, but coupled across channels and time frames to allow our approach to model interactions between channels and frames and vectorize across frequency. To do so, we use a recurrent neural network (RNN) where the weights ϕ are shared across all frequency bins, but we maintain separate state $\psi_k[\tau]$ per frequency. The inputs of our optimizer at frequency k are $\xi_k[\tau] = \{\nabla_k[\tau], \mathbf{u}_k[\tau], \mathbf{d}_k[\tau], \mathbf{y}_k[\tau]\}$, where $\nabla_k[\tau]$ is the gradient of the optimizee with respect to θ_k . The outputs of our optimizer are the update $\Delta_k[\tau]$ and the updated internal state $\psi_k[\tau + 1]$, resulting in

$$(\Delta_k[\tau], \psi_k[\tau + 1]) = g_\phi(\xi_k[\tau], \psi_k[\tau]) \quad (22)$$

$$\theta_k[\tau + 1] = \theta_k[\tau] + \Delta_k[\tau]. \quad (23)$$

Our design is in contrast to LMS-, NLMS-, RMSProp-like optimizers that have no state (e.g. LMS) or minimal state dynamics (e.g. NLMS, RMSProp). In addition, these conventional optimizers as well as other learned optimizers [69] typically apply updates independently per element. For a more complete comparison of optimizers, please see Table I.

To define our RNN in more detail, we use a small network composed of a linear layer, nonlinearity, and two Gated Recurrent Unit (GRU) layers, followed by two additional linear layers with nonlinearities, where all layers are complex-valued. Prior to the input, we 1) compute the error $\mathbf{e}_k[\tau] = \mathbf{d}_k[\tau] - \mathbf{y}_k[\tau]$ 2) stack all input signals $\xi_k[\tau]$ with $\mathbf{e}_k[\tau]$ into a single vector, and 3) approximately whiten the input vector magnitudes element-wise via

$$\ln(1 + |\nabla|)e^{j\angle \nabla}, \quad (24)$$

to reduce the dynamic range and facilitate training, but keep the phases unchanged. This pre-processing was found useful in several previous works [60], [69], although previous work used explicit clipping, which we found unnecessary.

2) *Loss*: We examine two meta losses $\mathcal{L}_M(\cdot)$ to learn our optimizer parameters ϕ . First, we define the frequency-domain *frame independent* loss

$$\mathcal{L}_M = \ln \frac{1}{L} \sum_{\tau}^{\tau+L} E[|\mathbf{d}[\tau] - \mathbf{y}[\tau]|^2], \quad (25)$$

where $\mathbf{d}[\tau]$ and $\mathbf{y}[\tau]$ are the desired and estimated frequency-domain signal vectors. Intuitively, to compute this loss for a given optimizer g_ϕ , we unroll (20) for a time horizon of L time frames, compute the average frequency-domain mean-squared error over L frames, and then take the logarithm to reduce the dynamic range, which we found to empirically improve learning. This loss ignores the temporal order of AF updates and optimizes for filter coefficients that are unaware of any downstream STFT processing. The basic idea of independently accumulating time-step losses is common [69].

Second, we define the time-domain *frame accumulated* loss

$$\mathcal{L}_M = \ln E[|\bar{\mathbf{d}}[\tau] - \bar{\mathbf{y}}[\tau]|^2], \quad (26)$$

$$\bar{\mathbf{d}}[\tau] = \text{cat}(\mathbf{d}[\tau], \mathbf{d}[\tau + 1], \dots, \mathbf{d}[\tau + L]) \in \mathbb{R}^{RL \times M} \quad (27)$$

$$\bar{\mathbf{y}}[\tau] = \text{cat}(\mathbf{y}[\tau], \mathbf{y}[\tau + 1], \dots, \mathbf{y}[\tau + L]) \in \mathbb{R}^{RL \times M} \quad (28)$$

where $\mathbf{d}[\tau]$ and $\mathbf{y}[\tau]$ are the time-domain desired and estimated responses. Intuitively, to compute this loss for a given

Algorithm 1 Training algorithm.

```

function FORWARD( $g_\phi, \psi, h_\theta, \mathbf{u}, \mathbf{d}$ )
  for  $\tau \leftarrow 0$  to  $L$  do                                 $\triangleright$  Unroll
     $\mathbf{u}[\tau], \mathbf{d}[\tau] \leftarrow \text{STFT}(\mathbf{u}[\tau], \mathbf{d}[\tau])$        $\triangleright$  Forward STFT
     $\mathbf{y}[\tau] \leftarrow h_\theta(\mathbf{u}[\tau])$                        $\triangleright$  Save filter output
     $\mathbf{\underline{y}}[\tau] \leftarrow \text{STFT}^{-1}(\mathbf{y}[\tau])$                $\triangleright$  Inverse STFT
     $\mathcal{L} \leftarrow \|\mathbf{d}_m[\tau] - \mathbf{y}_m[\tau]\|^2$                $\triangleright$  AF frame loss
     $\nabla[\tau] \leftarrow \text{GRAD}(\mathcal{L}, \theta)$                  $\triangleright$  Filter gradient
    for  $k \leftarrow 0$  to  $K$  do                             $\triangleright$  Apply update per freq
       $\xi_k[\tau] \leftarrow \{\nabla_k[\tau], \mathbf{u}_k[\tau], \mathbf{d}_k[\tau], \mathbf{y}_k[\tau]\}$ 
       $(\Delta_k[\tau], \psi_k[\tau + 1]) \leftarrow g_\phi(\xi_k[\tau], \psi_k[\tau])$ 
       $\theta_k[\tau + 1] \leftarrow \theta_k[\tau] + \Delta_k[\tau]$ 
     $\bar{\mathbf{y}} \leftarrow \text{VEC}(\mathbf{y})$                              $\triangleright$  Concatenate
  return  $\bar{\mathbf{y}}, \psi, h_\theta$ 

function TRAIN( $\mathcal{D}$ )
   $\phi \leftarrow [79]$  init
  while  $\phi$  not CONVERGED do                             $\triangleright$  Train loop
     $\mathbf{u}, \mathbf{d} \leftarrow \text{SAMPLE}(\mathcal{D})$                    $\triangleright$  Sample signals
     $\theta, \psi \leftarrow \mathbf{0}, \mathbf{0}$                          $\triangleright$  Init filter and optimizer state
    for  $n \leftarrow 0$  to end do                           $\triangleright$  Loop across long signal
       $\bar{\mathbf{u}}, \bar{\mathbf{d}} \leftarrow \text{NEXTL}(\mathbf{u}, \mathbf{d})$            $\triangleright$  Get next  $L$  frames
       $\bar{\mathbf{y}}, \psi, h_\theta \leftarrow \text{FORWARD}(g_\phi, \psi, h_\theta, \bar{\mathbf{u}}, \bar{\mathbf{d}})$ 
       $\mathcal{L}_M \leftarrow \ln E[\|\bar{\mathbf{d}} - \bar{\mathbf{y}}\|^2]$                $\triangleright$  Meta loss
       $\nabla \leftarrow \text{GRAD}(\mathcal{L}_M, \phi)$                  $\triangleright$  Optimizer gradient
       $\phi[n + 1] \leftarrow \text{METAOPT}(\phi[n], \nabla)$        $\triangleright$  Update opt
    return  $\phi$                                            $\triangleright$  Return best  $\phi$ 

```

optimizer g_ϕ , we run (20) for a time horizon of L frames, concatenate the sequence of time-domain outputs and target signals to form longer signals, then compute the time-domain MSE loss, and take the logarithm. While both losses use the same time-horizon, the frame accumulated loss allows us to model boundaries between adjacent updates and implicitly learn updates that are STFT consistent [75]. To the best of our knowledge, our frame accumulated loss is novel.

D. Learning the Optimizer

To learn an optimizer g_ϕ from data, we solve (21) using standard deep learning tools (i.e. JAX [76], [77]). We use truncated backpropagation through time (TBPTT) [78] with a stochastic gradient descent optimizer, Adam, that we call our meta optimizer. We show a simplified form of our training algorithm in Alg. 1 using our frame accumulated loss and a batch size of one, where STFT is an OLA or OLS processor, GRAD returns the gradient of the first argument with respect to the second, SAMPLE randomly samples signals from a dataset \mathcal{D} , and NEXTL grabs the next L time buffers from a longer signal. In practice, we also use batching.

In more detail, we train g_ϕ until the mean SNR metric on the validation fold of a dataset \mathcal{D} has not improved for four epochs. We halve the step size after an epoch with no improvement and define an epoch as 10 passes through the dataset with a batch size of 64. We have a hard stop for training at 100 epochs. From initial experimentation, we note the choice of the meta-optimizer and meta-optimizer parameters have large impact on performance. We initialize ϕ via [79]

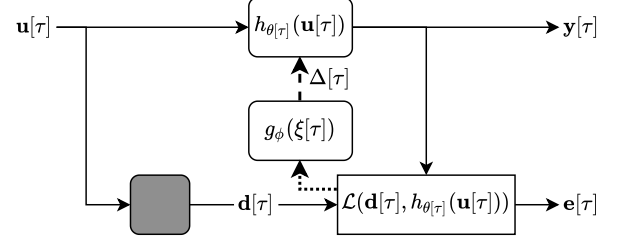


Fig. 1: System identification block diagram. System inputs are fed to both the adaptive filter and the true system (shaded box). The adaptive filter is updated to mimic the true system.

and, when using Adam, we found it was important to use a small learning of 10^{-4} and a large momentum term of .99. To help stabilize training we use gradient clipping with a clipping value of 10. We use identical g_ϕ configurations for each task where the input size of g_ϕ is set to $M \cdot B \cdot 4$, and the output size is $M \cdot B$. All intermediate layer sizes are set to 32 and use separate ReLU nonlinearities for real and imaginary.

To validate our approach, we use this algorithm to develop meta-learned AFs for five audio tasks including system identification, acoustic echo cancellation, equalization, single/multi-channel dereverberation, and beamforming in Section IV, Section V, Section VI, Section VII, and Section VIII, respectively and compare against conventional methods. For our first task, we also ablate key design decisions and then lock a single configuration for all remaining tasks and experiments.

IV. SYSTEM IDENTIFICATION ABLATIONS

A. Problem Formulation

For our first task, we train a meta-AF to perform online system identification (ID). We seek to estimate the transfer function between an audio source and a microphone over time as shown in Fig. 1, a task commonly used for room acoustics and head-related transfer function measurements for virtual and augmented reality. To do so, we model the unknown system (e.g. acoustic room) with a linear frequency-domain filter h_θ (optimizee architecture), then inject an input signal \mathbf{u} into the system, measure the recorded output target \mathbf{d} , and adapt the filter weights θ using our learned Meta-ID AF, g_ϕ .

B. Experimental Design

We 1) ablate key design decisions of our AF optimizer architecture and loss in Section IV-C and 2) study the robustness of our approach to modeling errors by changing the AF and true system order at test time in Section IV-D. For evaluation metrics, we use the segmental SNR (SNR_d) between the desired and estimated signals in dB. We compute this per-frame as,

$$\text{SNR}_d(\mathbf{d}[\tau], \mathbf{\underline{y}}[\tau]) = 10 \cdot \log_{10} \left(\frac{\|\mathbf{d}[\tau]\|^2}{\|\mathbf{d}[\tau] - \mathbf{\underline{y}}[\tau]\|^2} \right), \quad (29)$$

where higher is better. When averaging, we discard silent frames using an energy-threshold voice-activity detector (VAD). We train g_ϕ via Algorithm 1 using a single GPU

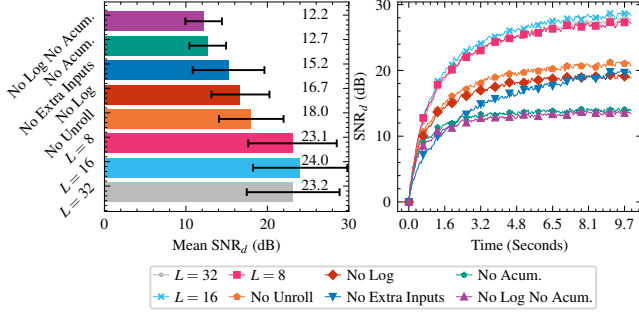


Fig. 2: Optimizer design decision ablation results. Using an accumulated log-loss leads to our best model. RLS-like inputs are also useful. While the exact value of L is not critical, larger is better.

to adapt an OLS filter with a rectangular window size of $N = 2048$ samples and hop size of $R = 1024$ samples on 16 kHz audio.

For training data, we created a system id dataset by convolving the far-end speech recordings from the single-talk portion of the Microsoft AEC Challenge [80] with room impulse responses (RIRs) from [81]. At test time, we truncate all RIRs to 1024 taps.

C. Optimizer Design Results & Discussion

We show the impact of our learned optimizer design in Fig. 2 by modifying one aspect of our final design (light blue, x) at a time including the optimizer loss, optimizer inputs, and unroll length (L) of the optimizer loss. After this, we fix these values for all remaining experiments and do not perform any further tuning except changing the dataset used for training and using different checkpoints caused by early stopping on validation performance. In contrast, we re-tune all conventional optimizer baselines for all subsequent tasks on validation sets.

1) *Loss Function*: First, we compare our selected frame accumulated loss model (light blue, x) to the frame accumulated loss without log scaling (orange, pentagon) as well as the frame independent loss with (green, star) and without log scaling (purple, up-triangle). As shown, either frame accumulated loss has the single largest effect on average and segmental SNR_d and yields an astounding 11.3/11.8 dB improvement compared to the frame independent loss. When we listen to the estimated response, we found that the accumulated loss introduces fewer artifacts and perceptually sounds better. Finally, when we compare the linear vs. log scaled accumulated loss, the log scaling provides a 7.3 dB improvement. Thus, we fix the optimizer loss to be (26).

2) *Input Features*: Having selected the optimizer loss, we now compare the model inputs in Fig. 2. We compare two options 1) setting the optimizer input to be only the gradient $\xi_k[\tau] = \{\nabla_k[\tau]\}$ for an LMS-like learned optimizer (dark blue, down triangle) and 2) setting the optimizer to be the full signal set $\xi_k[\tau] = \{\nabla_k[\tau], \mathbf{u}_k[\tau], \mathbf{d}_k[\tau], \mathbf{y}_k[\tau]\}$ for our selected RLS-like learned optimizer (light blue, x). As shown, the inputs have the second largest effect on SNR_d and using

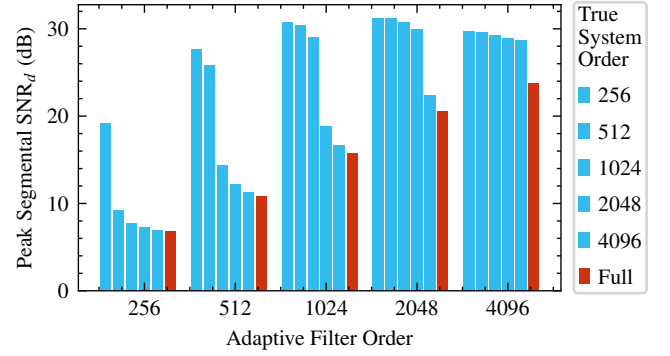


Fig. 3: Evaluating the effect of different true system orders and adaptive filter orders. Our learned AFs can operate well across a variety of linear system orders, even when training is restricted to systems of a fixed length (1024 taps).

the full signal set yields a notable 8.8 dB improvement. Thus, we set the input to be the full signal set.

3) *AF Unroll*: With the optimizer loss and inputs fixed, we evaluate four different values of AF unroll length, $L = 2, 8, 16, 32$, where L is the number of time-steps over which the optimizer loss is computed in (26). Intuitively, a larger unroll introduces less truncation bias but may be more unstable during training due to exploding or vanishing gradients. Also, the case where $L = 2$ corresponds to no unroll, otherwise the optimizer loss will not be a function of the optimizer parameters and yield a zero gradient. As shown, for no unroll $L = 2$ (red, diamond), we get a reduction of the SNR_d by nearly 6 dB compared to our best model, suggesting a model that is temporally unaware. When selecting the unroll between 8, 16, 32, however, there is a small (< 1 dB) overall effect. That said, we find that longer unroll values work better in challenging scenarios but take longer to train. As a result, we select an unroll length of 16, as it represents a good trade-off between performance and training time. Note, the unroll length only effects training and is not used at test time.

D. System Order Modeling Error Results & Discussion

Given our fixed set of optimizer and meta-optimizer parameters from above, we evaluate the robustness of our Meta-ID AF to modeling errors by studying what happens when we use an optimizee filter that is too short or too long compared to the true system. We do so by testing a learned optimizer with 1) optimizee filter lengths between 256 and 4096 taps and 2) held-out signals with true filter lengths between 256 and 4096, as well as full length systems (up to 32,000 taps).

Results are shown in Fig. 3. We measure performance by computing the peak segmental SNR_d score, which captures converged performance. As expected, when the adaptive filter order is equal to or greater than the true system order, we achieve SNRs above 25 dB. It is interesting to note that our learned AF was only ever trained on optimizee filters with an order of 1024 and full length true system. This experiment suggests our learned optimizers can generalize to new optimizee filter orders and fit them effectively.

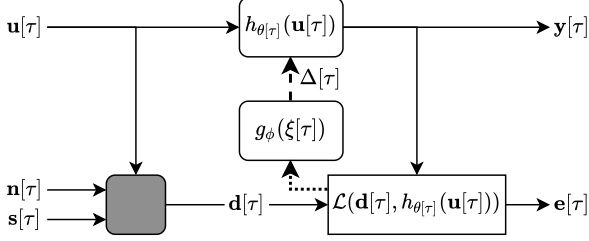


Fig. 4: AEC block diagram. System inputs are fed to the adaptive filter and true system (shaded box). The adaptive filter is updated to mimic the true system. The desired response can be noisy due to near-end noise and speech ($\mathbf{n}[\tau], \mathbf{s}[\tau]$).

V. ACOUSTIC ECHO CANCELLATION ABLATION

A. Problem Formulation

In our second task, we train a meta-AF for acoustic echo cancellation (AEC). The goal of AEC is to remove the far-end echo from a near-end signal for voice communication by mimicking a time-varying transfer function as show in Fig. 4. The far-end refers to signal transmitted to a local listener and the near-end is captured by a local mic. We model the unknown transfer function between the speaker and mic with a linear frequency-domain filter h_θ , measure the noisy response \mathbf{d} which includes the input signal \mathbf{u} , noise \mathbf{n} , and near-end speech \mathbf{s} , and adapt the filter weights θ using our learned Meta-AEC AF, g_ϕ . The time-domain signal model is $\mathbf{d}[t] = \mathbf{u}[t] * \hat{\mathbf{w}} + \mathbf{n}[t] + \mathbf{s}[t]$. The AF loss is the MSE between the near-end and the predicted response.

B. Experimental Design

We compare our approach to LMS, NLMS, RLS, a Kalman filter (KF) model [11], and Speex [12] for a variety of acoustic echo cancellation scenarios. Our scenarios, in increasing difficulty, include single-talk, double-talk, double-talk with a path change, and noisy double-talk with nonlinearities. Single-talk refers to the case where only the far-end input signal \mathbf{u} is active. Double-talk refers to the case where both the far-end signal \mathbf{u} and near-end talker signal \mathbf{s} are active at the same time. A path change refers to the case where the true system transfer function is abruptly changed (e.g. during a phone call). Nonlinearities refer to the case where the true system is not strictly linear (e.g. harmonic loudspeaker distortion). We train a new g_ϕ for each scene type (no tuning) and tune all baselines for each scene type.

We measure echo cancellation performance using segmental echo-return loss enhancement (ERLE) [82] and short-time objective intelligibility (STOI) [83]. Segmental ERLE is

$$\text{ERLE}(\mathbf{d}_u[\tau], \mathbf{y}[\tau]) = 10 \cdot \log_{10} \left(\frac{\|\mathbf{d}_u[\tau]\|^2}{\|\mathbf{d}_u[\tau] - \mathbf{y}[\tau]\|^2} \right), \quad (30)$$

where \mathbf{d}_u is the noiseless system response and higher values are better. When averaging, we discard silent frames using an energy-threshold VAD. In scenes with near-end speech, we use $\text{STOI} \in [0, 1]$ to measure the preservation of near-end

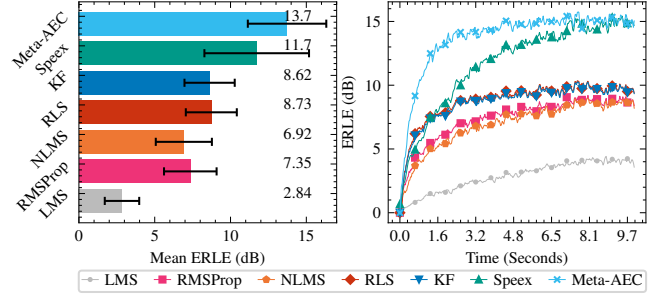


Fig. 5: AEC single-talk performance. Meta-AEC converges rapidly and has similar steady-state performance to Speex. We use this same legend for all AEC plots.

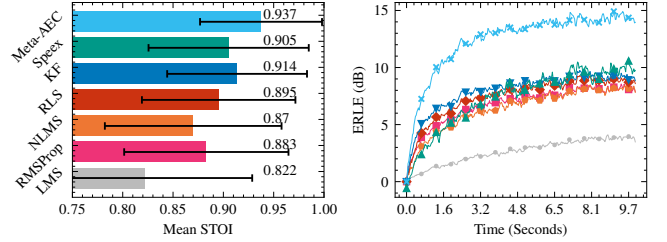


Fig. 6: AEC double-talk performance. Meta-AEC converges faster and has better peak performance than any baseline while preserving near-end speech quality.

speech quality. Higher STOI values are better. We train g_ϕ via Algorithm 1 using one or two GPUs, which took at most 48 hours. We use an OLS filter with a window size of $N = 2048$ samples and a hop of $R = 1024$ samples on 16 kHz audio. In double-talk scenarios, we use the noisy near-end, \mathbf{d} as the target and do not use oracle cancellation results (such as \mathbf{d}_u).

With respect to datasets for single-talk, double-talk, and double-talk with path-change experiments, we re-mix the synthetic fold of [80] with impulse responses from [81]. We partition [81] into non-overlapping train, test, and validation folds and set the signal-to-echo-ratio randomly between $[-10, 10]$ with uniform distribution. To simulate a scene change, we splice two files such that the change occurs randomly between seconds four and six. For the noisy double-talk with nonlinearity experiments, we use the synthetic fold of [80]. We apply a random circular shift to all files, each ten seconds long. In total, there are 9000 training, 500 validation, and 500 test files.

C. Results & Discussion

Overall, we find that our approach significantly outperforms all previous methods in all scenarios, but has a larger advantage in harder scenes—more details discussed below.

1) *Single-Talk*: Our approach (light blue, x) exhibits strong single-talk convergence and matches Speex (green, up triangle) at ≈ 15 dB, as shown in Fig. 5. Though, our Meta-AEC converges faster, reaching steady-state ≈ 3 seconds sooner. This leads to an average performance improvement of 1.7 dB.

2) *Double-Talk*: Our method (light blue, x) significantly outperforms all baselines for double-talk in all metrics as well as convergence speed as shown in Fig. 6. Our approach is

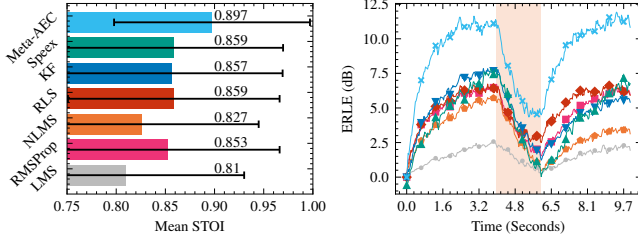


Fig. 7: AEC double-talk with a path change (shaded region) performance. Our approach re-converges rapidly with high speech quality.

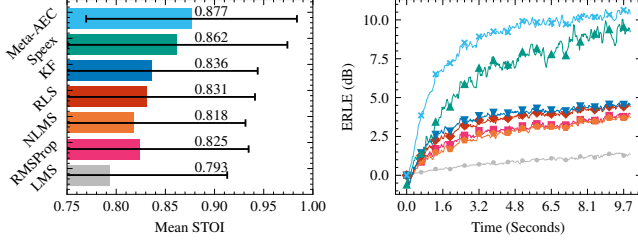


Fig. 8: AEC noisy double-talk with nonlinearities performance. Meta-AEC learns to compensate for the nonlinearity.

able to remove ≈ 5 dB more signal energy while scoring 0.023 higher in STOI. This result is striking as it is typically necessary to freeze adaptation via double-talk detection as found in both the KF model (dark blue, diamond) and Speex (green, up triangle). Our approach, however, has no explicit double-talk detector. As such, we hypothesize our method automatically learn how to adapt through double-talk in a completely autonomous fashion.

3) *Double-Talk with Path Change*: Our method (light blue, x) is able to more robustly handle double-talk with path changes compared to other methods as shown in Fig. 7. Similar to straight double-talk, our approach effectively learns how to deal with adverse conditions (i.e. a path change) without explicit supervision, converging and reconverging in ≈ 2.5 seconds, with $\approx .04$ better mean STOI. All other algorithms similarly struggle, even Speex (green, up triangle), which has explicit self-resetting and dual-filter logic.

4) *Noisy Double-Talk with Nonlinearities*: When we evaluate scenes with noise and nonlinearities to simulate loudspeaker distortion, we find that our Meta-AEC approach (light blue, x) continues to outperform all other conventional methods as shown in Fig. 8. That is, our peak-performance is ≈ 1 dB above the nearest baseline. In STOI, Meta-AEC scores .015 above Speex. We hypothesize that our approach effectively learns to compensate for the signal model inaccuracy, even if we only use a linear filter.

5) *Computational Complexity*: Our full learned AF has a single CPU core real-time factor (RTF) (computation/time) of ≈ 0.16 , and 64 ms latency (OLS hop size). Our optimizer network alone has $\approx 14K$ complex-valued parameters and single CPU core RTF of ≈ 0.14 . While this performance is already sufficient, we hypothesize that our RTF performance can be reduced further with better optimized code.

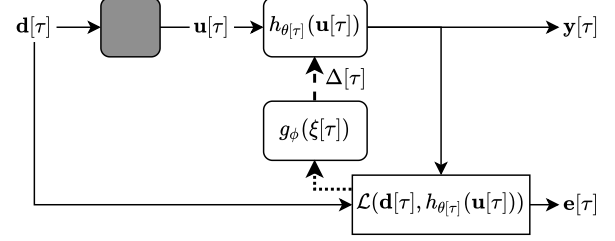


Fig. 9: Inverse modeling block diagram. System outputs are fed to the adaptive filter. The adaptive filter is continually updated to invert the unknown system (shaded box).

VI. EQUALIZATION ABLATION

A. Problem Formulation

For our third task, we train a meta-AF for the inverse modeling task of equalization (EQ). Here, our goal is to estimate the inverse of an unknown transfer function, while only observing input and outputs of the forward system, as shown in Fig. 9 and common for loudspeaker tuning. We model the unknown inverse transfer function with a linear frequency-domain filter h_{θ} , measure the noisy response \mathbf{d} to an input signal \mathbf{u} , and adapt the filter weights θ using our learned Meta-EQ AF g_{ϕ} . The AF loss is the MSE between the true and predicted responses.

B. Experimental Design

We compare our Meta-EQ approach to LMS, NLMS, and RLS for the task of performing frequency equalization. Additionally, we ablate the equalization filtering mechanics for two cases: constrained and unconstrained filters (optimizee architecture modifications). In the constrained case, we set h_{θ} to use standard OLS. However, in the unconstrained case, we set h_{θ} to use aliased OLS where $\mathbf{Z}_w = \mathbf{I}_K$. We are interested test if we can implicitly learn constraint-aware update rules without the need of explicit anti-aliasing. We train a new g_{ϕ} for each case (no tuning) and tune all baselines for each case.

We measure performance with signal SNR_d , and system SNR_w . We define these as

$$\text{SNR}_d(\mathbf{d}, \mathbf{y}) = 10 \cdot \log_{10} \left(\frac{\|\mathbf{d}\|^2}{\|\mathbf{d} - \mathbf{y}\|^2} \right) \quad (31)$$

$$\text{SNR}_w(\hat{\mathbf{w}}^{-1}, \mathbf{w}^{-1}) = 10 \cdot \log_{10} \left(\frac{\|\hat{\mathbf{w}}^{-1}\|^2}{\|\hat{\mathbf{w}}^{-1} - \mathbf{w}^{-1}\|^2} \right) \quad (32)$$

respectively, where higher is better. We compute SNR_w using the inverse system magnitude, which ignores the phase. We train g_{ϕ} via Algorithm 1 on one GPU, which took at most 36 h. We use an OLS filter with a window size of $N = 1024$ samples and a hop of $R = 512$ samples on 16 kHz audio.

To construct the equalization dataset, we use speech from the DAPS dataset [84]. We construct input/output pairs by applying [5, 15] equalizer effects from the sox library with $c \in [1, 8]$ kHz, $g \in [-18, 18]$, and $q \in [.1, 10]$. All values are sampled uniformly at random to produce 16,384 train, 2048 validation and 2048 test signals, all 5 seconds long. At train

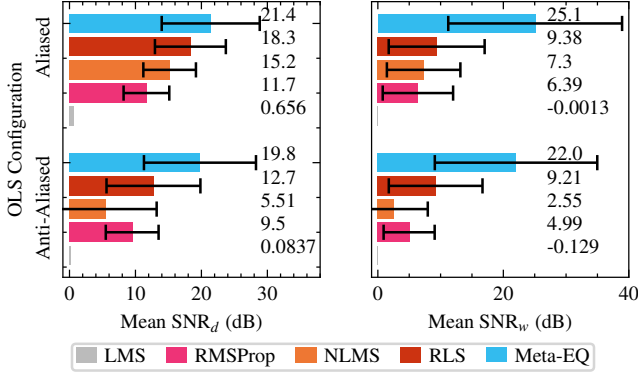


Fig. 10: Equalization results for signal (SNR_d) and system (SNR_w) SNR. Meta-EQ performance is the least impacted by constraints.

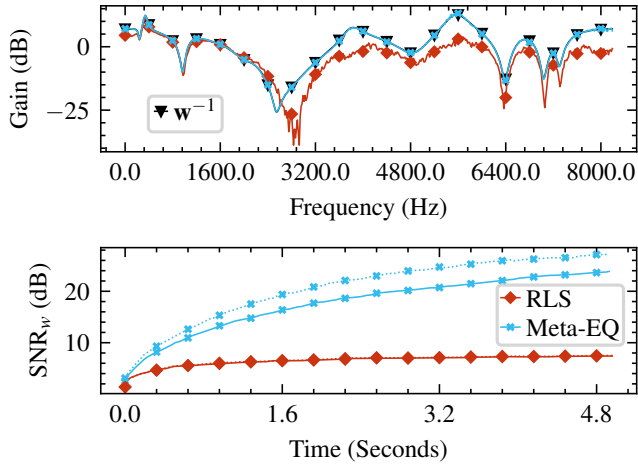


Fig. 11: Comparison of true and estimated systems over time. The Meta-EQ system rapidly fits to the correct inverse model. The top plot shows an example system and the bottom shows SNR_w over time across the test set.

and validation time, the true system is longer than the adaptive filter. At test time, we truncate the response to 512 taps.

C. Results & Discussion

We find our approach (blue, solid) outperforms LMS, RMSProp, NLMS, and RLS for our equalization task by a noticeable margin as shown in Fig. 10 and further verify with a qualitative analysis plot in Fig. 11.

1) *Constrained vs Unconstrained*: For the unconstrained case, our method outperforms RLS in SNR_d by 3.1 dB and by 15.72 dB in SNR_w. When we look at the constrained case, the performance for all models is degraded. Interestingly, however, our performance is proportionally degraded the least. We hypothesize that our approach learns to perform updates which are aware of the constraint.

2) *Temporal Performance Analysis*: We display final system and convergence results in Fig. 11. Our Meta-EQ model finds better solutions more rapidly than RLS. RLS diverged ≈ 150 times but Meta-EQ never did. We believe the RLS values are low since, it was tuned to maximize SNR_d.

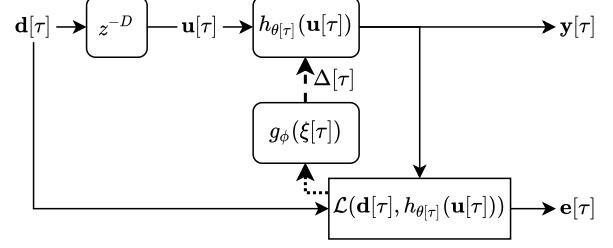


Fig. 12: Prediction block diagram. A buffer of past inputs are used to estimate a future, unknown signal. The delay, z^{-D} signifies a delay by D frames.

3) *Computational Complexity*: Our full learned AF has a single CPU core RTF of ≈ 0.24 , and 32 ms latency. Our optimizer network alone has $\approx 14K$ complex-valued parameters and single CPU core RTF of ≈ 0.19 .

VII. DEREVERBERATION ABLATION

A. Problem Formulation

For our fourth task, we train a meta-AF to perform dereverberation via multi-channel linear prediction (MCLP) or the weighted prediction error (WPE) formulation as is commonly used for speech-to-text pre-processing. The WPE formulation is based on the idea being able to predict the reverberant part of a signal from a linear combination of past samples, most commonly in the frequency-domain [23], [24] and shown as a block diagram in Fig. 12. Using our method, we use a multi-channel linear frequency-domain filter h_θ and adapt the filter weights θ using a learned AF g_ϕ to minimize the normalized MSE AF loss below.

Assuming an array of M microphones, we estimate a dereverberated signal with a linear model via

$$\hat{\mathbf{d}}_{\text{km}}[\tau] = \mathbf{d}_{\text{km}}[\tau] - (\mathbf{w}_{\text{km}}[\tau]^H \odot \tilde{\mathbf{u}}[\tau]) \mathbf{1}_{BM \times 1} \quad (33)$$

where $\hat{\mathbf{d}}_{\text{km}}[\tau] \in \mathbb{C}$ is the current dereverberated signal estimate at frequency k and channel m , $\mathbf{d}_{\text{km}}[\tau] \in \mathbb{C}$ is the input microphone signal, $\mathbf{w}_{\text{km}}[\tau]^H \in \mathbb{C}^{1 \times BM}$ is a per frequency filter with B time frames and M channels flattened into a vector, and $\tilde{\mathbf{u}}[\tau] = \tilde{\mathbf{d}}_k[\tau - D] \in \mathbb{C}^{1 \times BM}$ is a running buffer of $\mathbf{d}_{\text{km}}[\tau]$, delayed by D frames.

We then minimize a per channel and frequency loss

$$\mathcal{L}(\hat{\mathbf{d}}_{\text{km}}[\tau], \lambda_k[\tau]) = \frac{\|\hat{\mathbf{d}}_{\text{km}}[\tau]\|^2}{\lambda_k^2[\tau]}, \quad (34)$$

$$\lambda_k^2[\tau] = \frac{1}{M(B+D)} \sum_{n=\tau-B-D}^{\tau} \mathbf{d}_k[n]^H \mathbf{d}_k[n], \quad (35)$$

where $\lambda_k^2[\tau]$ is a running average estimate of the signal power and $\mathbf{d}_k[\tau] \in \mathbb{C}^{M \times 1}$. We use this formation and loss within our framework to perform online multi-channel dereverberation or Meta-WPE and focus on dereverberating a single, reference channel.

B. Experimental Design

We compare our Meta-WPE to frame-online NARA-WPE [28], an RLS based AF which uses the WPE formulation. We ablate the filter size and inputs across: $M = 1, 4, 8$ microphones (optimizee size and input modification). We seek to test if our method can scale from single- to multi-channel tasks without modification. We train a new g_ϕ for each M (no tuning). We measure performance with two metrics, segmental speech-to-reverberation ratio (SRR) [29] and STOI. SRR is a signal level metric and measures how much energy was removed from the signal. It is computed as,

$$\text{SRR}(\mathbf{d}_k[\tau], \hat{\mathbf{d}}_k[\tau]) = 10 \cdot \log_{10} \left(\frac{\|\hat{\mathbf{d}}_k[\tau]\|^2}{\|\mathbf{d}_k[\tau] - \hat{\mathbf{d}}_k[\tau]\|^2} \right), \quad (36)$$

where smaller values indicate more removed energy and better performance. STOI is computed between the output and the ground truth anechoic signal. We train g_ϕ via Algorithm 1 on two GPUs, which took at most 15h. We use an OLA filter with a Hann window size of $N = 512$ samples and a hop of $R = 256$ samples on 16 kHz audio. We fix the buffer size $B = 5$ taps and the delay to $D = 2$ frames.

We use the simulated REVERB challenge dataset [85]. The REVERB challenge contains echoic speech mixed with noise at 20 dB in small (T60=.25 sec), medium (T60=.5 sec) and large (T60=.7 sec) rooms at near and far distances. The array is circular with a diameter of 20 cm. Background noises are generally stationary. The dataset has 7861 training files, 1484 validation files, and 2176 test files.

C. Results & Discussion

We find our approach (blue, solid) outperforms NARA-WPE in SRR across all filter configurations, but is worse in STOI as shown in Fig. 13. We discuss this below.

1) *Overall and Temporal Performance:* As shown in Fig. 13, Meta-WPE (blue, solid) scores strongly on SRR, where our single-channel Meta-WPE model scores better than 4 and 8 channel NARA-WPE (green, dotted) models. However, as shown by STOI, the perceptual quality is poor. While Meta-WPE is solving the prediction more rapidly, as seen in segmental SRR, it is not doing so in a perceptual pleasing manner. This issue is known for WPE based dereverberation and studied in [29], where a variety of regularization tools are required to align the optimization objective with perceptually pleasing processing. We re-ran these experiments with a buffer of size $B = 10$ as well as with larger and smaller optimizer network capacity and found this trend was consistent. As a result, we conclude our approach is very effectively improving the online optimization of the target loss, but the loss itself needs to be changed to better align with perception.

2) *Computational Complexity:* The 4 channel learned AF has a single CPU core RTF of ≈ 0.47 , and 16ms latency. Our Meta-WPE optimizer network alone has $\approx 17K$ complex-valued parameters and single CPU core RTF of ≈ 0.38 .

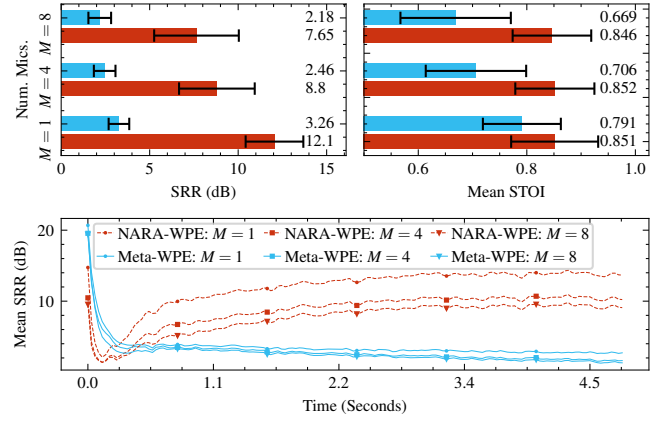


Fig. 13: Dereverberation performance in terms of SRR. Meta-WPE excels in SRR, a metric which measures energy removed. However, in STOI, Meta-WPE scores worse.

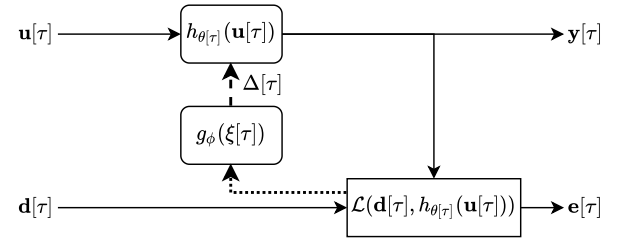


Fig. 14: Informed interference cancellation block diagram. An auxiliary signal is used as input to an adaptive filter which is fit to an alternate signal.

VIII. BEAMFORMING ABLATION

A. Problem Formulation

For our fifth and final task, we train a meta-AF for interference cancellation using the minimum variance distortionless response (MVDR) beamformer. The MVDR beamformer can be implemented as an AF using the generalized sidelobe canceller (GSC) [36] formulation and is commonly used for far-field voice communication and speech-to-text pre-processing. We depict a version of this problem setup in Fig. 14 and use a linear frequency-domain filter h_θ . We use the mixture \mathbf{d} as the target, informed input \mathbf{u} , and adapt the filter weights θ using our learned Meta-GSC AF g_ϕ and MSE AF loss.

Assuming an array of M microphones, we have the time-domain signal model for mic m via,

$$\mathbf{u}_m[t] = r_m[t] * \mathbf{s}[t] + \mathbf{n}_m[t] \quad (37)$$

where $\mathbf{u}_m[t] \in \mathbb{R}$ is the input signal, $\mathbf{n}_m[t] \in \mathbb{R}$ is the noise signal, $\mathbf{s}[t] \in \mathbb{R}$ is the true desired signal, and $r_m[t] \in \mathbb{R}$ is the impulse response from the source to mic m . In the time-frequency domain with a sufficiently long window, this can be rewritten as

$$\mathbf{u}_{km}[\tau] = \mathbf{r}_{km}[\tau] \mathbf{s}_k[\tau] + \mathbf{n}_{km}[\tau], \quad (38)$$

where k represents frequency and τ represents the short-time frame.

The GSC beamformer also assumes access to a steering vector, \mathbf{v}_k . Estimating the steering vector is well studied [36], and we use the normalized first principal component of the source covariance matrix,

$$\tilde{\mathbf{v}}_k[\tau] = \mathcal{P}(\Phi_k^{ss}[\tau]) \quad (39)$$

$$\mathbf{v}_k[\tau] = \tilde{\mathbf{v}}_k[\tau] / \tilde{\mathbf{v}}_{k0}[\tau] \quad (40)$$

where $\Phi_k^{ss}[\tau] \in \mathbb{C}^{M \times M}$ is an estimate of the covariance matrix for $\mathbf{s} \in \mathbb{C}^M$, $\mathcal{P}(\cdot)$ extracts the principal component and $\mathbf{v}_k[\tau] \in \mathbb{C}^M$ is the final steering vector. We assume access to \mathbf{s} when computing,

$$\Phi_k^{ss}[\tau] = \gamma \Phi_k^{ss}[\tau - 1] + (1 - \gamma)(\mathbf{s}_k[\tau]\mathbf{s}_k[\tau]^\top + \lambda \mathbf{I}_M) \quad (41)$$

where γ is a forgetting factor and λ is a regularization parameter. We then use the steering vector to estimate a blocking matrix $\mathbf{B}_k[\tau]$. The blocking matrix is orthogonal to the steering vector and can be constructed as

$$\mathbf{B}_k[\tau] = \begin{bmatrix} -[\mathbf{v}_{k1}[\tau], \dots, \mathbf{v}_{kM}[\tau]]^\top \\ \mathbf{v}_{k0}[\tau]^\top \\ \mathbf{I}_{M-1 \times M-1} \end{bmatrix} \in \mathbb{C}^{M \times M-1}. \quad (42)$$

The distortionless constraint is then satisfied by applying the GSC beamformer as

$$\hat{\mathbf{s}}_k[\tau] = (\mathbf{v}_k[\tau] - \mathbf{B}_k[\tau]\mathbf{w}_k[\tau])^\top \mathbf{u}_k[\tau] \quad (43)$$

where $\mathbf{w}_k[\tau] \in \mathbb{C}^{M-1}$ is the adaptive filter weight, and the desired response for the loss is $\mathbf{d}_k[\tau] = \mathbf{v}_k[\tau]^\top \mathbf{u}_k[\tau]$.

Our objective is to learn an optimizer g_ϕ that minimizes the AF MSE loss using this GSC filter implementation. By doing so, we learn an online, adaptive beamformer that listens in one direction and suppresses interferers from all others.

B. Experimental Design

We compare our Meta-GSC beamformer to LMS, NLMS, and RLS beamformers, in scenes with either diffuse or directional noise sources. We seek to test if our method can learn to process scenes with different spatial characteristics without modification. We train a new g_ϕ for each scene type (no tuning) and tune all baselines for each scene type. We measure performance using scale-invariant signal-to-distortion ratio (SI-SDR) [86] and STOI. SI-SDR is computed as,

$$\mathbf{a} = (\hat{\mathbf{s}}^\top \underline{\mathbf{s}}) / \|\underline{\mathbf{s}}\| \quad (44)$$

$$\text{SI-SDR}(\underline{\mathbf{s}}, \hat{\mathbf{s}}) = 10 \cdot \log_{10}(\|\underline{\mathbf{a}}\|^2 / \|\underline{\mathbf{a}} - \hat{\mathbf{s}}\|^2), \quad (45)$$

where larger values indicate better performance. STOI is computed between the output and desired speech signal. We train g_ϕ via Algorithm 1 on two-four GPUs, which took at most 24h. We use an OLA filter with a Hann window size of $N = 1024$ samples and a hop of $R = 512$ samples on 6 channel 16 kHz audio..

We use the CHIME-3 challenge proposed in [87], [88]. This dataset contains scenes with simulated speech and relatively diffuse noise sources in a multi-channel environment. The array is rectangular and has six microphones spaced around the edge of an iPad. There are 7138 training files, 1640 validation files, and 1320 test files. When running this dataset with directional sources we mix spatialized speech from one mixture with the spatialized speech from a random other mixture. We do not mix speech across folds.

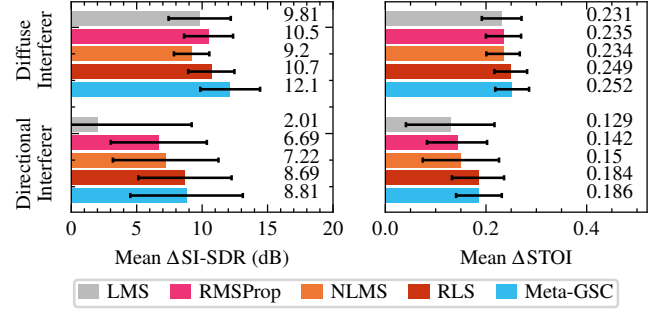


Fig. 15: Performance comparison across interferers. The directional noise is the most challenging and diffuse is the easiest.

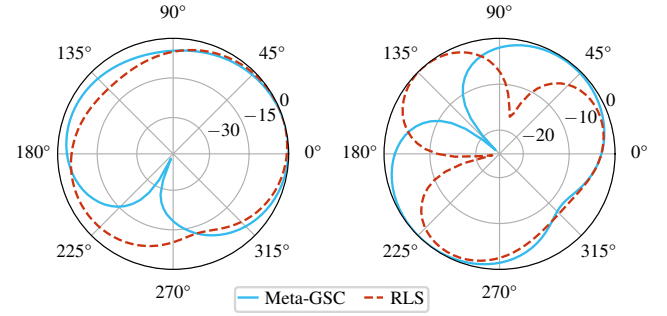


Fig. 16: Response plots at 500 Hz for a diffuse (left) and a directional (right) interferer.

C. Results and Discussion

We find our Meta-GSC outperforms LMS, RMSProp, NLMS, and RLS for average performance in Fig. 15 and in a qualitative analysis plot in Fig. 16.

1) *Diffuse Interferers*: The diffuse scenario tests the ability to suppress omnidirectional noise in a perceptually pleasant fashion. We show these comparisons in the top portion of Fig. 15. The input SI-SDR was -0.71 dB and the input STOI was 0.674 . Meta-GSC (blue, solid) performs 1.4 dB better and 0.003 than RLS (red, dotted) in SI-SDR and STOI, respectively. When we repeated this experiment with a larger optimizer model, results improve further.

2) *Directional Interferers*: The directional scenario tests the ability to suppress sources from one particular direction – typically achieved by steering nulls in the beam pattern. We show results in the bottom of Fig. 15. The input SI-SDR was -0.33 dB and the input STOI was 0.734 . Our Meta-GSC outperforms RLS by 0.12 dB in SI-SDR and 0.002 in STOI. We hypothesize Meta-GSC is learning to steer sharper nulls.

3) *Beam pattern Comparison*: We compute two beam plots for Meta-GSC and RLS modules, one with a diffuse interferer and one with a directional interferer. As expected, the models share the same look direction. However, our Meta-GSC method appears to steer more aggressive nulls as shown in Fig. 16. We used weights from the end of a scene.

4) *Computational Complexity*: Our Meta-GSC method has a single CPU core RTF of ≈ 0.54 , and 32 ms latency. The optimizer network alone has $\approx 14K$ complex-valued parameters and single CPU core RTF of ≈ 0.25 .

IX. DISCUSSION, FUTURE WORK, AND CONCLUSION

A. Discussion

When we review the cumulative results of our approach, we note several interesting observations. First, the performance of our meta-learned AFs is exceptional and compares very well to conventional optimizers across all tasks. Second, the performance difference between our meta-learned AFs and conventional AFs is larger for tasks that are traditionally more difficult to model by humans including AEC double-talk, AEC path changes, and diffuse interference cancellation. Third, we found that we could use a single configuration of our method for all five tasks, which significantly reduced our development time. This suggests that our learned AFs are a viable replacement of human-derived AFs for a variety of audio signal processing tasks and are most valuable for complex AF tasks that typically require more human engineering effort.

When we reflect on how our learned optimizers are able to achieve this success, we note two main likely reasons. First, and most obvious, our meta-learned AFs are *data-driven* and trained on a particular class of signals (e.g. speech, directional noise, etc). Thus, Meta-AF is limited by the capacity of our optimizer network and not signal modeling skill. Second, by framing AF development as a meta-learning problem, we effectively distill knowledge of our meta loss (e.g. our frame accumulated) into the AF loss and corresponding learned update rules, thus enabling us to learn AFs which optimize objectives that would be very difficult (e.g. our frame accumulated) or even impossible to develop manually (e.g. supervised losses, STOI, SISDR, etc).

B. Future Work

The field of meta-learning and meta-learned optimizers is young and has a bright future for signal processing applications. Future directions of research include improving training methods, non-linear optimizree filtering, optimizer architecture, and the optimizer/meta loss. Particularly promising avenues for future work including identifying better optimization losses and better filter representations for Meta-AF style optimization. Overall, we are optimistic that our Meta-AF approach can benefit from both adaptive filtering advances as well as deep learning progress and will be an exciting research topic.

C. Conclusion

We presented a general framework called Meta-AF to automatically develop adaptive filter update rules from data using meta-learning. To train, we use self-supervised training and thus never need any labeled data. To demonstrate the power of our framework, we tested it on all four canonical adaptive filtering architectures and five unique tasks including system identification, acoustic echo cancellation, equalization, dereverberation, and GSC-based beamforming – all using a single configuration trained on different datasets. In all cases, we were able to train high performing AFs, which outperformed conventional optimizers as well as certain state-of-the-art methods. We are excited about the future of deep learning combined with adaptive filters and hope our complete code release will stimulate further research and rapid progress.

REFERENCES

- [1] B. Widrow and S. D. Stearns, *Adaptive Signal Processing*. Prentice-Hall, 1985.
- [2] V. J. Mathews, *Circuits and Systems Tutorials: Adaptive polynomial filters*, 1991.
- [3] J.-S. Soo and K. K. Pang, “Multidelay block frequency domain adaptive filter,” *IEEE TASSP*, 1990.
- [4] S. S. Haykin, *Adaptive filter theory*. Pearson, 2008.
- [5] J. A. Apolinário, J. A. Apolinário, and R. Rautmann, “QRD-RLS adaptive filtering,” 2009.
- [6] L. R. Rabiner, B. Gold, and C. Yuen, *Theory and application of digital signal processing*. Prentice-Hall, 2016.
- [7] N. N. Schraudolph, “Local gain adaptation in stochastic gradient descent,” in *ICANN*, 1999.
- [8] S. L. Gay, “An efficient, fast converging adaptive filter for network echo cancellation,” in *IEEE Asilomar Conf. on Sig., Sys. and Comp.*, 1998.
- [9] J. Benesty, T. Gansler, D. R. Morgan, S. L. Gay, and M. M. Sondhi, *Advances in Network and Acoustic Echo Cancellation*. Springer, 2001.
- [10] E. Hänsler and G. Schmidt, *Acoustic echo and noise control: a practical approach*. John Wiley & Sons, 2005.
- [11] G. Enzner and P. Vary, “Frequency-domain adaptive Kalman filter for acoustic echo control in hands-free telephones,” *Elsevier Signal Processing*, vol. 86, no. 6, 2006.
- [12] J.-M. Valin, “On adjusting the learning rate in frequency domain echo cancellation with double-talk,” *IEEE TASLP*, 2007.
- [13] S. Malik and G. Enzner, “Online maximum-likelihood learning of time-varying dynamical models in block-frequency-domain,” in *IEEE ICASSP*, 2010.
- [14] F. Yang, G. Enzner, and J. Yang, “Frequency-domain adaptive Kalman filter with fast recovery of abrupt echo-path changes,” *IEEE SPL*, vol. 24, no. 12, 2017.
- [15] M. L. Valero and E. A. Habets, “Multi-microphone acoustic echo cancellation using relative echo transfer functions,” in *IEEE WASPAA*, 2017.
- [16] T. Haubner, A. Brendel, M. Elminshawi, and W. Kellermann, “Noise-robust adaptation control for supervised acoustic system identification exploiting a noise dictionary,” in *IEEE ICASSP*, 2021.
- [17] P. A. Nelson, H. Hamada, S. J. Elliott *et al.*, “Adaptive inverse filters for stereophonic sound reproduction,” *IEEE TSP*, vol. 40, no. 7, 1992.
- [18] P. A. Nelson, F. Orduna-Bustamante, and H. Hamada, “Inverse filter design and equalization zones in multichannel sound reproduction,” *IEEE TASLP*, vol. 3, no. 3, 1995.
- [19] M. Bouchard and S. Quednau, “Multichannel recursive-least-square algorithms and fast-transversal-filter algorithms for active noise control and sound reproduction systems,” *IEEE TSAP*, vol. 8, no. 5, 2000.
- [20] N. V. George and G. Panda, “Advances in active noise control: A survey, with emphasis on recent nonlinear techniques,” *Elsevier Signal Processing*, vol. 93, no. 2, 2013.
- [21] L. Lu, K.-L. Yin, R. C. de Lamare, Z. Zheng, Y. Yu, X. Yang, and B. Chen, “A survey on active noise control in the past decade—part i: Linear systems,” *Elsevier Signal Processing*, vol. 183, 2021.
- [22] —, “A survey on active noise control in the past decade—part ii: Nonlinear systems,” *Elsevier Signal Processing*, vol. 181, 2021.
- [23] T. Yoshioka, H. Tachibana, T. Nakatani, and M. Miyoshi, “Adaptive dereverberation of speech signals with speaker-position change detection,” in *IEEE ICASSP*, 2009.
- [24] T. Nakatani, T. Yoshioka, K. Kinoshita, M. Miyoshi, and B.-H. Juang, “Speech dereverberation based on variance-normalized delayed linear prediction,” *IEEE TASLP*, vol. 18, no. 7, 2010.
- [25] T. Yoshioka and T. Nakatani, “Generalization of multi-channel linear prediction methods for blind MIMO impulse response shortening,” *IEEE TASLP*, vol. 20, no. 10, 2012.
- [26] B. Li, T. N. Sainath, A. Narayanan, J. Caroselli, M. Bacchiani, A. Misra, I. Shafran, H. Sak, G. Pundak, K. K. Chin *et al.*, “Acoustic modeling for google home,” in *Interspeech*, 2017.
- [27] J. Caroselli, I. Shafran, A. Narayanan, and R. Rose, “Adaptive multichannel dereverberation for automatic speech recognition,” in *Inter-speech*, 2017.
- [28] L. Drude, J. Heymann, C. Boeddeker, and R. Haeb-Umbach, “NARA-WPE: A python package for weighted prediction error dereverberation in numpy and tensorflow for online and offline processing,” in *ITG-Symposium on Speech Communication*. VDE, 2018.
- [29] J. Wung, A. Jukić, S. Malik, M. Souden, R. Pichevar, J. Atkins, D. Naik, and A. Acero, “Robust multichannel linear prediction for online speech dereverberation using weighted householder least squares lattice adaptive filter,” *IEEE TSP*, vol. 68, 2020.

- [30] L. Griffiths and C. Jim, "An alternative approach to linearly constrained adaptive beamforming," *IEEE TAP*, vol. 30, no. 1, 1982.
- [31] O. Hoshuyama, A. Sugiyama, and A. Hirano, "A robust adaptive beamformer for microphone arrays with a blocking matrix using constrained adaptive filters," *IEEE TSP*, vol. 47, no. 10, 1999.
- [32] J. Chen, J. Benesty, and Y. Huang, "A minimum distortion noise reduction algorithm with multiple microphones," *IEEE TASLP*, vol. 16, no. 3, 2008.
- [33] M. Souden, J. Benesty, and S. Affes, "On optimal frequency-domain multichannel linear filtering for noise reduction," *IEEE TASLP*, vol. 18, no. 2, 2009.
- [34] Y. A. Huang and J. Benesty, "A multi-frame approach to the frequency-domain single-channel noise reduction problem," *IEEE TASLP*, vol. 20, no. 4, 2011.
- [35] S. Markovich-Golan, S. Gannot, and I. Cohen, "A sparse blocking matrix for multiple constraints GSC beamformer," in *IEEE ICASSP*, 2012.
- [36] S. Gannot, E. Vincent, S. Markovich-Golan, and A. Ozerov, "A consolidated perspective on multimicrophone speech enhancement and source separation," *IEEE TASLP*, vol. 25, no. 4, 2017.
- [37] A. N. Birkett and R. A. Goubran, "Acoustic echo cancellation using NLMS-neural network structures," in *IEEE ICASSP*, 1995.
- [38] A. B. Rabaa and R. Tourki, "Acoustic echo cancellation based on a recurrent neural network and a fast affine projection algorithm," in *IEEE IES*, 1998.
- [39] J. Malek and Z. Koldovský, "Hammerstein model-based nonlinear echo cancellation using a cascade of neural network and adaptive linear filter," in *IEEE IWAENC*, 2016.
- [40] S. Zhang and W. X. Zheng, "Recursive adaptive sparse exponential functional link neural network for nonlinear AEC in impulsive noise environment," *IEEE TNNLS*, 2017.
- [41] M. M. Halimeh, C. Huemmer, and W. Kellermann, "A neural network-based nonlinear acoustic echo canceller," *IEEE SPL*, 2019.
- [42] H. Zhang, K. Tan, and D. Wang, "Deep learning for joint acoustic echo and noise cancellation with nonlinear distortions," in *Interspeech*, 2019.
- [43] L. Ma, H. Huang, P. Zhao, and T. Su, "Acoustic echo cancellation by combining adaptive digital filter and recurrent neural network," *arXiv:2005.09237*, 2020.
- [44] A. Ivry, I. Cohen, and B. Berdugo, "Nonlinear acoustic echo cancellation with deep learning," *arXiv:2106.13754*, 2021.
- [45] J.-M. Valin, S. Tenneti, K. Helwani, U. Isik, and A. Krishnaswamy, "Low-complexity, real-time joint neural echo control and speech enhancement based on PercepNet," *arXiv:2102.05245*, 2021.
- [46] Y.-L. Zhou, Q.-Z. Zhang, X.-D. Li, and W.-S. Gan, "Analysis and DSP implementation of an ANC system using a filtered-error neural network," *Journal of Sound and Vibration*, vol. 285, no. 1-2, 2005.
- [47] T. Krukowicz, "Active noise control algorithm based on a neural network and nonlinear input-output system identification model," *Archives of Acoustics*, vol. 35, no. 2, 2010.
- [48] H. Zhang and D. Wang, "A deep learning approach to active noise control," in *Interspeech*, 2020.
- [49] —, "Deep anc: A deep learning approach to active noise control," *Neural Networks*, vol. 141, 2021.
- [50] K. Kinoshita, M. Delcroix, H. Kwon, T. Mori, and T. Nakatani, "Neural network-based spectrum estimation for online WPE dereverberation," in *Interspeech*, 2017.
- [51] J. Heymann, L. Drude, R. Haeb-Umbach, K. Kinoshita, and T. Nakatani, "Frame-online DNN-WPE dereverberation," in *IEEE IWAENC*, 2018.
- [52] L. Drude, C. Boeddeker, J. Heymann, R. Haeb-Umbach, K. Kinoshita, M. Delcroix, and T. Nakatani, "Integrating neural network based beamforming and weighted prediction error dereverberation," in *Interspeech*, 2018.
- [53] Z.-Q. Wang, G. Wichern, and J. Le Roux, "Convolutional prediction for reverberant speech separation," in *IEEE WASPAA*, 2021.
- [54] —, "Convolutional prediction for monaural speech dereverberation and noisy-reverberant speaker separation," *IEEE TASLP*, vol. 29, 2021.
- [55] H. Erdogan, J. R. Hershey, S. Watanabe, M. I. Mandel, and J. Le Roux, "Improved mvdr beamforming using single-channel mask prediction networks," in *Interspeech*, 2016.
- [56] J. Heymann, L. Drude, and R. Haeb-Umbach, "Neural network based spectral mask estimation for acoustic beamforming," in *IEEE ICASSP*, 2016.
- [57] K. Qian, Y. Zhang, S. Chang, X. Yang, D. Florencio, and M. Hasegawa-Johnson, "Deep learning based speech beamforming," in *IEEE ICASSP*, 2018.
- [58] Z. Zhang, Y. Xu, M. Yu, S.-X. Zhang, L. Chen, and D. Yu, "ADL-MVDR: All deep learning MVDR beamformer for target speech separation," in *IEEE ICASSP*, 2021.
- [59] T. Haubner, A. Brendel, and W. Kellermann, "End-to-end deep learning-based adaptation control for frequency-domain adaptive system identification," *arXiv:2106.01262*, 2021.
- [60] J. Casebeer, N. J. Bryan, and P. Smaragdis, "Auto-DSP: Learning to optimize acoustic echo cancellers," in *IEEE WASPAA*, 2021.
- [61] J. Casebeer, J. Donley, D. Wong, B. Xu, and A. Kumar, "NICE-beam: Neural integrated covariance estimators for time-varying beamformers," *arXiv:2112.04613*, 2021.
- [62] R. Scheibler and M. Togami, "Surrogate source model learning for determined source separation," in *IEEE ICASSP*, 2021.
- [63] R. S. Sutton, "Adapting bias by gradient descent: An incremental version of delta-bar-delta," in *AAAI*, 1992.
- [64] A. R. Mahmood, R. S. Sutton, T. Degris, and P. M. Pilarski, "Tuning-free step-size adaptation," in *IEEE ICASSP*, 2012.
- [65] J. Schmidhuber, "Learning to control fast-weight memories: An alternative to dynamic recurrent networks," *Neural Computation*, 1992.
- [66] I. Bello, B. Zoph, V. Vasudevan, and Q. V. Le, "Neural optimizer search with reinforcement learning," in *ICML*, 2017.
- [67] D. Ha, A. Dai, and Q. V. Le, "Hypernetworks," in *ICLR*, 2017.
- [68] C. Finn, P. Abbeel, and S. Levine, "Model-agnostic meta-learning for fast adaptation of deep networks," in *ICML*, 2017.
- [69] M. Andrychowicz, M. Denil, S. G. Colmenarejo, M. W. Hoffman, D. Pfau, T. Schaul, B. Shillingford, and N. de Freitas, "Learning to learn by gradient descent by gradient descent," in *NeurIPS*, 2016.
- [70] O. Wichrowska, N. Maheswaranathan, M. W. Hoffman, S. G. Colmenarejo, M. Denil, N. Freitas, and J. Sohl-Dickstein, "Learned optimizers that scale and generalize," in *ICML*, 2017.
- [71] L. Metz, N. Maheswaranathan, J. Nixon, D. Freeman, and J. Sohl-Dickstein, "Understanding and correcting pathologies in the training of learned optimizers," in *ICML*, 2019.
- [72] T. Chen, W. Zhang, Z. Jingyang, S. Chang, S. Liu, L. Amini, and Z. Wang, "Training stronger baselines for learning to optimize," in *NeurIPS*, 2020.
- [73] A. V. Oppenheim and R. W. Schaffer, *Digital signal processing*. Prentice-Hall, 1975.
- [74] G. Hinton, N. Srivastava, and K. Swersky, "Neural networks for machine learning lecture 6a overview of mini-batch gradient descent," 2012.
- [75] J. Le Roux, N. Ono, and S. Sagayama, "Explicit consistency constraints for STFT spectrograms and their application to phase reconstruction," in *Interspeech*, 2008.
- [76] J. Bradbury, R. Frostig, P. Hawkins, M. J. Johnson, C. Leary, D. Maclaurin, and S. Wanderman-Milne, "JAX: composable transformations of Python+ NumPy programs, 2018," URL <http://github.com/google/jax>, 2020.
- [77] T. Hennigan, T. Cai, T. Norman, and I. Babuschkin, "Haiku: Sonnet for JAX," 2020. [Online]. Available: <http://github.com/deepmind/dm-haiku>
- [78] P. J. Werbos, "Backpropagation through time: what it does and how to do it," *IEEE*, 1990.
- [79] M. Wolter and A. Yao, "Complex gated recurrent neural networks," in *NeurIPS*, 2018.
- [80] R. Cutler, A. Saabas, T. Parnamaa, M. Purin, H. Gamper, S. Braun, K. Sorensen, and R. Aichner, "ICASSP 2022 acoustic echo cancellation challenge," in *IEEE ICASSP*, 2022.
- [81] T. Ko, V. Peddinti, D. Povey, M. L. Seltzer, and S. Khudanpur, "A study on data augmentation of reverberant speech for robust speech recognition," in *IEEE ICASSP*, 2017.
- [82] G. Enzner, H. Buchner, A. Favrot, and F. Kuech, "Acoustic echo control," in *Academic press library in signal processing*. Elsevier, 2014, vol. 4.
- [83] C. H. Taal, R. C. Hendriks, R. Heusdens, and J. Jensen, "An algorithm for intelligibility prediction of time-frequency weighted noisy speech," *IEEE TASLP*, vol. 19, no. 7, 2011.
- [84] G. J. Mysore, "Can we automatically transform speech recorded on common consumer devices in real-world environments into professional production quality speech?—a dataset, insights, and challenges," *IEEE SPL*, vol. 22, no. 8, 2014.
- [85] K. Kinoshita, M. Delcroix, S. Gannot, E. A. Habets, R. Haeb-Umbach, W. Kellermann, V. Leutnant, R. Maas, T. Nakatani, B. Raj *et al.*, "A summary of the REVERB challenge: state-of-the-art and remaining challenges in reverberant speech processing research," *EURASIP Journal on Advances in Signal Processing*, vol. 2016, no. 1, 2016.
- [86] J. Le Roux, S. Wisdom, H. Erdogan, and J. R. Hershey, "SDR—half-baked or well done?" in *IEEE ICASSP*, 2019.
- [87] J. Barker, R. Marxer, E. Vincent, and S. Watanabe, "The third CHiME speech separation and recognition challenge: Dataset, task and baselines," in *IEEE ASRU*, 2015.
- [88] —, "The third CHiME speech separation and recognition challenge: Analysis and outcomes," *Computer Speech & Language*, vol. 46, 2017.